Consequences of high-x proton size fluctuations in small collision systems at RHIC

D. McGlinchey,[1] J. L. Nagle,[1] and D. V. Perepelitsa[2]

[1] *University of Colorado, Boulder, Colorado 80309, USA*

[2] *Physics Department, Brookhaven National Laboratory, Upton, New York 11973-5000, USA*

(Dated: March 23, 2016)

Recent measurements of jet production rates at large transverse momentum (p_T) in the collisions of small projectiles with large nuclei at RHIC and the LHC indicate that they have an unexpected relationship with estimates of the collision centrality. One compelling interpretation of the data is that it captures an x_p-dependent decrease in the average interaction strength of the nucleon in the projectile undergoing a hard scattering. A weakly interacting or "shrinking" nucleon in the projectile strikes fewer nucleons in the nucleus, resulting in a particular pattern of centrality-dependent modifications to high-p_T processes. We describe a simple one-parameter geometric implementation of this picture within a modified Monte Carlo Glauber model tuned to d+Au jet data, and explore two of its major consequences. First, the model predicts a particular projectile-species dependence to the centrality dependence at high-x_p, opposite to that expected from an energy loss effect. Second, we find that some of the large centrality dependence observed for forward di-hadron production in d+Au collisions at RHIC may arise from the physics of the "shrinking" projectile nucleon, in addition to impact parameter-dependent shadowing or saturation effects at low nuclear-x. We conclude that analogous measurements in recently collected p+Au and ^{3}He+Au collision data at RHIC can provide a unique test of these predictions.

PACS numbers: 25.75.Gz

arXiv:1603.06607v1 [nucl-th] 21 Mar 2016

I. INTRODUCTION

Recent measurements of jet production at large transverse momentum (p_T) in the collisions of small projectiles (protons and deuterons) with large target nuclei have revealed an unexpected relationship between the jet rate and soft-particle production signatures understood to be related to the collision geometry. The rate of inclusive jet production was analyzed in $\sqrt{s_{NN}} =$ 200 GeV deuteron–gold (d+Au) [1] and $\sqrt{s_{NN}} =$ 5.02 TeV proton–lead (p+Pb) [2] collisions at the Relativistic Heavy Ion Collider (RHIC) and Large Hadron Collider (LHC), respectively, as a function of the collision *centrality*, an experimental handle on the geometric configuration of the projectile–nucleus collision system.

In these measurements, the rate of jet production in projectile–nucleus (generically, p+A) collisions was compared to the expectation derived by scaling the jet rate in individual nucleon–nucleon (N+N) collisions by the additional degree of nuclear overlap. The deviation from this expectation is traditionally quantified with a nuclear modification factor,

$$R_{p+\mathrm{A}} = \left(dN^{p+\mathrm{A}}/dp_T\right) / \left(T_{p+\mathrm{A}} d\sigma^{p+p}/dp_T\right). \qquad (1)$$

In Eq. 1, the numerator is the per-event yield in p+A collisions, while the denominator is the jet production cross-section in p+p collisions scaled by the nuclear overlap in p+A collisions, $T_{p+\mathrm{A}}$. Schematically, the denominator may also be understood as the product of the per-N+N collision yield and N_{coll}, the mean number of N+N collisions in a projectile–nucleus collision, giving $T_{p+\mathrm{A}} d\sigma^{p+p}/dp_T = N_{\mathrm{coll}}(\sigma_{NN}^{-1} d\sigma^{p+p}/dp_T)$ where σ_{NN} is the inelastic N+N cross-section. $R_{p+\mathrm{A}}$ may be evaluated for different selections on jet kinematics and, as described below, for different selections on p+A event classes.

When measured in minimum bias (MB)—i.e., centrality-integrated—collisions, the total rate of jet production was found to be comparable to this expectation ($R_{p+\mathrm{A}} \approx 1$), and any small deviations from this were generally in line with global analyses of the modifications to the parton densities in nuclei [3], and with minimal energy loss in the initial stages of the collision [4].

On the other hand, jet rates were also evaluated under different selections on the event centrality, which in both measurements was characterized using the total particle activity at large pseudorapidity in the nucleus-going direction. A Glauber model [5] was used to describe the distribution of N_{coll} values in p+A collision geometries and phenomenological models [6] of the relationship between N_{coll} and the centrality signal were used to determine the mean N_{coll} in each centrality selection [7, 8].

Figure 1 shows the measured $R_{p+\mathrm{A}}$ for d+Au collisions ($R_{d+\mathrm{Au}}$) in each of the reported centrality ranges. In central collisions, those associated with small centrality values (0–20%) and large N_{coll} values, the jet rate was found to be systematically lower than this expectation ($R_{p+\mathrm{A}} < 1$). In peripheral collisions, those associated with large centrality values (60–88%) and small N_{coll} values, the jet rate was instead systematically higher than the expectation ($R_{p+\mathrm{A}} > 1$). In both selections, the scale of the deviations from $R_{p+\mathrm{A}} = 1$ generally increased with jet p_T. While the behavior in central events may be seen as consistent with a modest jet energy loss in the initial or final states [4, 9], the enhanced rate of jet production in peripheral events is difficult to understand within traditional energy loss pictures. Furthermore, the centrality-dependent modifications are much

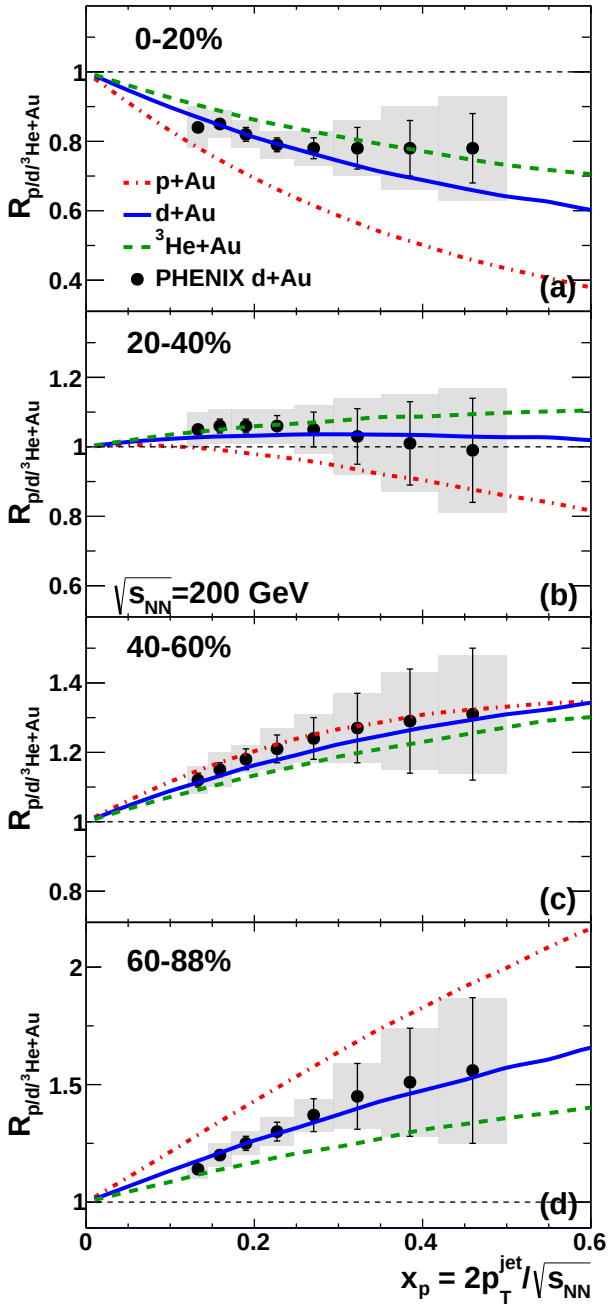

FIG. 1. (Color Online) The calculated $R_{p+\mathrm{A}}$ as a function of x_p in each centrality bin for $p/d/^3$He+Au compared to the measured $R_{d+\mathrm{Au}}$ of jets in d+Au collisions at $\sqrt{s_{NN}} = 200$ GeV [1].

larger than what could be expected from an impact parameter dependence of the nuclear parton densities [10]. Finally, while an increase in the soft-particle production rate for N+N collisions with a hard-scattering is expected to bias centrality-dependent measurements of jet production, measurements of this correlation in p+p collisions [7, 11] and estimates of their impact in p+A collisions [7, 12, 13] demonstrate that this effect is small and in the opposite direction of the observed modifications.

The magnitude of these modifications can be also explored through the ratio of the N_{coll}-scaled per-event yield between central and peripheral p+A collisions,

$$R_{CP} = \frac{1/N_{\mathrm{coll}}^{\mathrm{central}}\; dN^{\mathrm{central}}/dp_T}{1/N_{\mathrm{coll}}^{\mathrm{peripheral}}\; dN^{\mathrm{peripheral}}/dp_T} = \frac{R_{p+\mathrm{A}}^{\mathrm{central}}}{R_{p+\mathrm{A}}^{\mathrm{peripheral}}}. \quad (2)$$

While the $R_{p+\mathrm{A}}$ is necessary to understand the absolute modifications with respect to the expectation from N+N collisions, the smaller experimental systematic uncertainties associated with an R_{CP} measurement allow it to quantify the relative modification between two p+A event classes more precisely.

A unifying way to understand the central, peripheral, and MB data together is to hypothesize that jet production is unmodified, but the soft-particle production used to estimate centrality is affected in events with high-p_T jets. In such an explanation, the overall jet rate is unaffected when integrated among all types of p+A collisions and is merely redistributed among the centrality classes, naturally explaining the observed modifications. Furthermore, the modifications in the data appear only to depend on the longitudinal momentum of the hard-scattered parton in the projectile, x_p, and on no other kinematic variable. While the $R_{p+\mathrm{A}}$ modifications at RHIC and the LHC appear at very different p_T^{jet} ranges, they are at similar ranges in x_p. Additionally, the ATLAS $R_{p+\mathrm{A}}$ analysis demonstrated that the results at multiple rapidity selections have a universal dependence only on x_p [2].

A compelling underlying description of such an effect is that it arises from color fluctuations in the internal configuration of the projectile nucleon. Since hadrons are composite objects, their Fock space description is a distribution over quark-gluon configurations with varying properties. In hadronic collisions, the different possible internal configurations result in event-by-event fluctuations in the effective interaction cross-section [14, 15]. For the hadronic configurations with a large-x_p parton available for a hard scattering, the average cross-section is expected to decrease on general grounds since, for example, such configurations have a fewer than average number of partons [16]. Thus, when passing through a large nucleus, these weakly interacting or geometrically "shrinking" configurations interact with fewer nucleons than an average-sized configuration, resulting in a relative decrease in the N_{coll} distribution for these events with a large-x_p scattering parton.

Such an interpretation of the data was first proposed by the authors of Ref. [17] (and see references therein). Other authors have described empirical models in which a similar effect can be achieved through a depletion of the longitudinal energy of the projectile remnant after the removal of a high-x_p parton [18] or from an overall x_p-dependent suppression in the soft particle multiplicity per-N+N collision [19]. We do not discuss the merits of these approaches here, but rather focus on the proton

color fluctuation picture, since it has a simple geometric interpretation which can be implemented in modern Monte Carlo Glauber (MC-Glauber) approaches.

In this paper, we argue that a systematic scan of centrality-dependent hard process rates in small collision systems at RHIC as a function of the projectile nucleus mass number (A=1,2,3) can better explore the underlying physics mechanisms. Specifically, this can be performed with measurements of high-p_T jet or particle production rates in high-luminosity p+Au, d+Au, and helium–gold (^{3}He+Au) collision data taken in 2014, 2008, and 2015, respectively. On general grounds, a suppression of the $R_{p+\mathrm{A}}$ in central p+A collisions which arises from energy loss should become stronger with increasing projectile mass number, since the amount of nuclear material and thus path length increases. On the other hand, a suppression of the central $R_{p+\mathrm{A}}$ (and enhancement of the peripheral $R_{p+\mathrm{A}}$) which arises from the shrinking of a high-x_p hard-scattered projectile nucleon should generally decrease with increasing projectile mass number, since the N_{coll} contributed by the other nucleons in the projectile which did not undergo the hard scattering would be unaffected. Thus, the unique capability of RHIC to deliver $p/d/^3$He+Au collisions at the same energy can serve as a novel way to constrain the underlying phenomenon.

In addition, we argue that the effects of proton color fluctuations at large projectile-x_p contributes to the observed centrality dependence of forward hadron and di-hadron production rates in d+Au collisions at RHIC [20–23]. The strong centrality dependence observed in these collisions has been previously taken to be evidence of non-linear QCD effects at small nuclear-x. However, high-p_T particle production in this kinematic regime is dominated by $x_p > 0.1$, meaning that proton color fluctuations affect the apparent centrality dependence of hard scattering rates. We demonstrate that this effect should be accounted for in order to quantify the modifications from remaining nuclear effects.

Our paper is organized as follows. In Section II, we implement a one-parameter model of an x_p-dependent decrease in the N+N interaction strength in a MC-Glauber approach and describe its application to the centrality frameworks used by the PHENIX Collaboration. In Section III, we give the predictions of our model, after tunning to recent d+Au measurements, for the $R_{p+\mathrm{A}}$ and R_{CP} in p+Au and ^{3}He+Au collisions. In Section IV we discuss the consequences of this picture for interpretations of forward di-hadron production measurements at RHIC. We finish with a discussion and summary in Section V.

II. MODEL

This section describes a simple geometric interpretation of an x_p-dependence of the nucleon-nucleon interaction strength for the hard scattering projectile nucleon within a Glauber model picture of p+A collisions. The model is discussed in Sec. II A, and its implementation in a MC-Glauber simulation and application to the centrality frameworks used by experiments is detailed in Sec. II B.

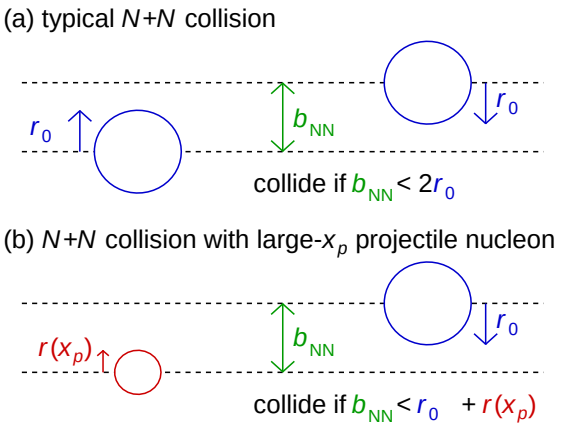

FIG. 2. (Color Online) Schematic picture of a nucleon-nucleon collision for the case of (a) an unmodified projectile nucleon and (b) a projectile nucleon whose radius depends on x_p.

A. Geometric picture of shrinking proton

Our analysis models the hypothesis that in a high-energy p+A collision in which a large-x_p parton in the projectile undergoes a hard-scattering, the nucleon–nucleon interaction cross-section $\sigma_{_{NN}}$ between the projectile nucleon and nucleons in the nucleus is reduced. Classically, the collision cross-section σ for two hard spheres with radii r_1 and r_2 is given by $\sigma = \pi(r_1 + r_2)^2$. By analogy, for a projectile nucleon with a large-x_p hard-scattered parton, let the interaction radius, r, be dependent on the x of the projectile parton, x_p, and given by $r(x_p)$. The interaction radius for all other nucleons is given by $r_0 = \sqrt{\sigma_{_{NN}}/4\pi}$. A schematic view of colliding nucleons in the modified and unmodified case is shown in Fig. 2. As argued above, at large x_p ($\gtrsim 0.1$), $r(x_p) < r_0$ and decreases with increasing x_p. We model $r(x_p)$ phenomenologically as a decreasing exponential function characterized by one parameter β,

$$r(x_p) \equiv \exp(-\beta x_p) r_0. \tag{3}$$

This functional form decreases smoothly and continuously with x_p without introducing many parameters. The resulting nucleon–nucleon cross-section, $\sigma(x_p)$, is therefore x_p-dependent and is given by

$$\sigma(x_p) \equiv \pi(r_0 + r(x_p))^2 = \frac{1}{4}\left(1 + \exp(-\beta x_p)\right)^2 \sigma_{_{NN}}. \tag{4}$$

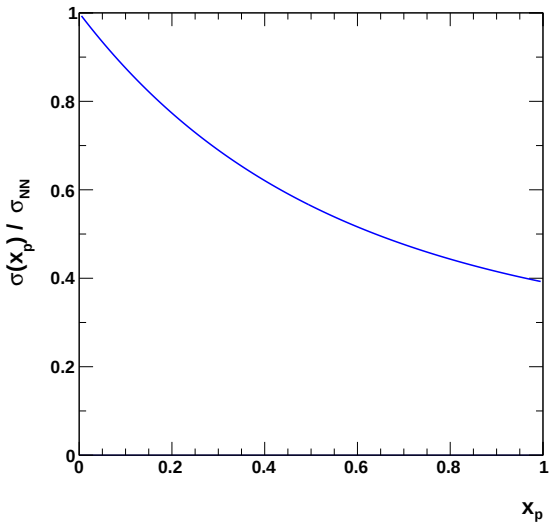

FIG. 3. Ratio of the modified nucleon-nucleon cross section $\sigma(x_p)$ to the nominal value $\sigma_{_{NN}}$, as a function of the momentum fraction in the projectile nucleon (x_p).

In our treatment, the high-x_p configuration is taken to be frozen throughout the duration of the collision. Furthermore, the interaction radius of every other nucleon in the p+A system is unmodified. Thus, the interaction cross-section between any pair of nucleons which do not contain the large-x_p projectile nucleon is $\sigma_{_{NN}}$.

In our analysis, β was ultimately determined to be $1.38^{+0.09}_{-0.07}$ by implementing this shrinking nucleon picture in a Glauber Monte Carlo analysis, convolving with the centrality framework used by PHENIX, and fitting to the d+Au centrality-dependent jet data in Ref. [1]. These steps are described in detail in the next sections. The resulting x_p-dependent cross-section as a fraction of the nominal $\sigma_{_{NN}}$ is shown in Fig. 3. Schematically, the value of $\beta = 1.38$ implies that for projectile nucleon configurations with $x_p \sim 0.2$ (~ 0.6), $\sigma(x_p)$ is reduced by $\sim 25\%$ ($\sim 50\%$) relative to $\sigma_{_{NN}}$.

B. Application to experimental centrality models

To determine the effects of the shrinking proton on experimentally measured centrality-dependent hard-scattered yields, the consequences of Eq. 4 are implemented in the MC-Glauber analysis and centrality framework used by the PHENIX experiment in Ref. [7]. The PHOBOS Glauber Monte Carlo code [24] is used to simulate the possible range of $p/d/^3$He+Au collision geometries. In the MC-Glauber approach, the transverse positions of the nucleons in both the target and projectile nuclei are sampled on an event-by-event basis, with each nucleon required to have a minimum separation distance of 0.4 fm from all others. We use the default prescriptions present in the PHOBOS MC-Glauber for describing the radial distributions of nuclei in ^{3}He and Au nuclei. To model the deuteron, the Hulthén form is chosen [25].

In all three collision systems, the nucleon-nucleon cross section $\sigma_{_{NN}}$ is chosen to be 42 mb at the center-of-mass energy $\sqrt{s} = 200$ GeV. For each simulated event, the projectile nuclei are displaced in the transverse plane by a random impact parameter, and $N_{\rm coll}$ is determined by projecting nucleons along straight line (longitudinal) trajectories. Any projectile-target nucleon pair is treated as having interacted if their transverse impact parameter is smaller than the sum of the interaction radii. For unmodified N+N interactions, this condition is $b_{_{NN}} < 2r_0 = \sqrt{\sigma_{_{NN}}/\pi}$. After many simulated events, a given collision system can be described by a probability distribution over the number of N+N collisions, $P(N_{\rm coll})$.

In the PHENIX experiment, classes of p+A collisions are selected indirectly through the total charge, Q, measured in the beam–beam counter (BBC), situated at $-3.9 < \eta < -3.0$, i.e. in the gold-going direction. A given range of Q values is related to a set of p+A collisions by assuming that all collisions with a given value of $N_{\rm coll}$ produce a distribution over the charge given by a negative binomial distribution (NBD) with $N_{\rm coll}$ dependent parameters. A NBD over Q can be described by a mean μ and positive exponent κ, with probability mass function defined by[1]

$$NBD(Q;\mu,\kappa) = \left(1+\frac{\mu}{\kappa}\right)^{-\kappa} \frac{(\kappa+Q-1)!}{Q!(\kappa-1)!} \left(\frac{\mu}{\mu+\kappa}\right)^{Q}. \quad (5)$$

The parameters are taken to grow linearly in $N_{\rm coll}$, $\mu(N_{\rm coll}) = \mu N_{\rm coll}$ and $\kappa(N_{\rm coll}) = \kappa N_{\rm coll}$. That is, the distribution at fixed $N_{\rm coll}$ is an $N_{\rm coll}$-fold convolution of an elemental distribution with parameters μ and κ.

Since the MB trigger condition is not fully efficient for peripheral p+A events, the efficiency ϵ_{MB} at a given value of Q is modeled with the following two-parameter functional form,

$$\epsilon_{MB}(Q) \equiv 1 - \exp\left((Q/p_0)^{p_1}\right), \quad (6)$$

where p_0 and p_1 are determined from fits to data. Thus, for a given input distribution $P(N_{\rm coll})$, the resulting per-event MB dN/dQ distribution measured in PHENIX is given by

$$\frac{dN}{dQ} \equiv \frac{\epsilon_{MB}(Q)}{\epsilon_{MB,tot}} \left(\sum_{N_{\rm coll}} P(N_{\rm coll}) NBD(Q;\mu N_{\rm coll}, \kappa N_{\rm coll})\right), \quad (7)$$

[1] This definition differs from the one in Ref. [7] only in the $(1+\mu/\kappa)^{-\kappa}$ normalization term, which in this paper ensures that $\sum_Q NBD(Q) = 1$ explicitly.

TABLE I. The negative binomial distribution parameters μ and κ, trigger efficiency parameters p_0 and p_1, and total MB trigger efficiency $\epsilon_{MB,tot}$ used to characterize the centrality in each collision system by the PHENIX experiment [7, 26].

System	μ	κ	p_0	p_1	$\epsilon_{MB,tot}$
p+Au	3.14	0.47	1.076	0.602	84%
d+Au	3.04	0.46	0.897	0.612	88%
^{3}He+Au	2.91	0.55	1.221	0.510	84%

where $\epsilon_{MB,tot}$ is the MB trigger efficiency for all p+A collisions and serves as an overall normalization constant. The resulting distribution is then divided into a number of centiles according to $\epsilon_{MB,tot}$.

The charge distribution $dN^{\rm hard}/dQ$ for events with a generic hard process (one expected to obey $N_{\rm coll}$-scaling) is identical to Eq. 7 but with an $N_{\rm coll}$-weighting within the summation,

$$\frac{dN^{\rm hard}}{dQ} \equiv \frac{\epsilon_{MB}(Q)}{\epsilon_{MB,tot}} \left(\sum_{N_{\rm coll}} N_{\rm coll} P(N_{\rm coll}) NBD(Q;\mu N_{\rm coll}, \kappa N_{\rm coll}) \right). \quad (8)$$

Since the performance of the BBC system was found by PHENIX to have a small run-dependence, the μ and κ parameters are slightly different for each collision system. These small performance differences, in addition to the different $N_{\rm coll}$ distributions, also result in collision-system dependent values of p_0, p_1 and $\epsilon_{MB,tot}$. All five parameters are summarized in Table I. For brevity, we denote the most peripheral selection for all collision systems as 60–88%, even though it is really 60–84% for p+Au and ^{3}He+Au collisions.

In this paper, our emphasis is on exploring the projectile-species dependence of shrinking projectile nucleon effects. We found that the simple modification to the PHOBOS MC Glauber simulation described above was sufficient for this purpose. However, other authors have raised the importance of improved modeling of the nucleon-nucleon correlations in the nucleus or of the localization of high-x partons in the transverse core of nucleons [27]. While including these effects could slightly alter the quantitative results, they would not change our essential conclusions.

III. RESULTS AND DISCUSSION

To determine the nuclear modification factors $R_{p+\rm A}$ and R_{CP} arising from proton color fluctuations, the simulated $p/d/^3$He+Au events are re-analyzed under the hypothesis of a shrinking projectile nucleon. For each simulated $p/d/^3$He+Au event, the number of soft nucleon–nucleon interactions is recalculated by modifying $\sigma_{_{NN}}$ for the hard-scattered projectile nucleon to be $\sigma(x_p)$. In d+Au and ^{3}He+Au collisions, the affected projectile nucleon is chosen at random in each simulated event. In each event, this results in a modified number of total N+N collisions $N_{\rm coll}{}'$, which is a function of x_p. Operationally, in Eq. 8 the $N_{\rm coll}$-dependent centrality signal for events with a hard scattering is modified via

$$NBD(Q;\mu N_{\rm coll}, \kappa N_{\rm coll}) \rightarrow NBD(Q;\mu N'_{\rm coll}(x_p), \kappa N'_{\rm coll}(x_p)), \quad (9)$$

yielding an x_p-dependent Q distribution for hard-scattered events, $dN^{\rm hard}/dQ(x_p)$. This analysis is repeated over a wide range of x_p values in small steps of x_p. The resulting $R_{p+\rm A}$ values as a function of x_p are obtained for each centrality selection (exclusive Q range) by evaluating the ratio of the integral of the modified $dN^{\rm hard}/dQ(x_p)$ distribution to the unmodified one,

$$R_{p+\rm A}(x_p) \equiv \int_{cent} dQ \frac{dN^{\rm hard}}{dQ}(x_p) \Big/ \int_{cent} dQ \frac{dN^{\rm hard}}{dQ}. \quad (10)$$

By construction, for MB (i.e. centrality—or Q—integrated) collisions, the $R_{p+\rm A}$ is unity. The resulting x_p-dependent R_{CP} values are ratios of the $R_{p+\rm A}$ values in the corresponding centrality bins, $R_{CP}(x_p) = R^{\rm central}_{p+\rm A}(x_p)/R^{\rm peripheral}_{p+\rm A}(x_p)$.

Figures 1 and 4 show the resulting $R_{p+\rm A}$ and R_{CP} values as a function of x_p for the p+Au, d+Au and ^{3}He+Au systems. The calculations are compared to the d+Au centrality-dependent jet $R_{d+\rm Au}$ and R_{CP} measurement by PHENIX [1], under the assumption that the production of jets at $y = 0$ corresponds to typical x_p values given by

$$x_p(p_T^{\rm jet}) = 2p_T^{\rm jet}/\sqrt{s_{_{NN}}}. \quad (11)$$

The value of $\beta = 1.38^{+0.09}_{-0.07}$ was determined by fitting the calculated d+Au R_{CP} in the most central-to-peripheral selection (0–20%/60–88%) to that in data as a function of x_p. The figures show only the central value β result as the uncertainty band is small relative to the uncertainty in the data. Our one-parameter model is sufficient to describe the x_p-dependence of the measured jet $R_{p+\rm A}$ and R_{CP} values in d+Au collisions.

The same value of β is used to calcuate the $R_{p+\rm A}$ and R_{CP} as a function of x_p for p+Au and ^{3}He+Au collisions at RHIC, where centrality-dependent hard-process rates have not yet been reported. A clear ordering between the collision systems is observed in each centrality selection, with the R_{CP} for ^{3}He+Au collisions less suppressed than that for d+Au collisions, which is itself less suppressed than that for p+Au collisions. The predicted modifications for p+Au collisions are particularly large, showing a 50% suppression in central collisions and a factor of two enhancement in peripheral collisions, at $x_p \sim 0.4 - 0.5$.

This ordering is a direct consequence of the presence of one (two) additional projectile nucleons in d+Au

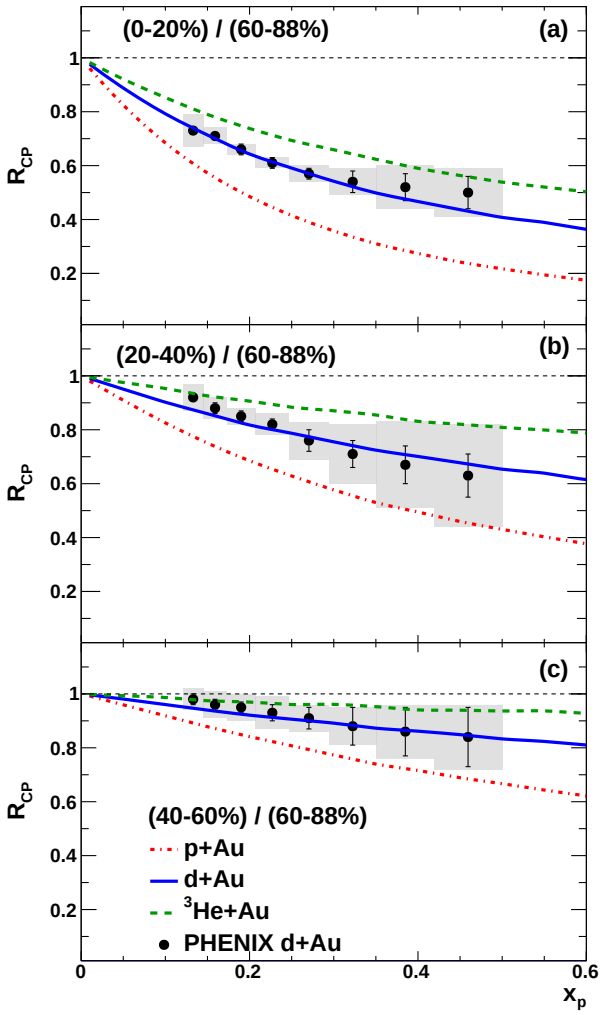

FIG. 4. (Color Online) The calculated R_{CP} as a function of x_p in each centrality bin compared to the measured R_{CP} of jets in d+Au collisions at $\sqrt{s_{NN}} = 200$ GeV [1].

(^{3}He+Au) collisions compared to the single projectile nucleon in p+Au collisions. The additional projectile nucleons, which did not undergo a hard-scattering and which do not generally have a large-x_p parton, have an unmodified interaction cross–section σ_{NN}. Thus, the centrality signal generated by soft nucleon–nucleon collisions in which these additional projectile nucleons participate is unmodified. This dilutes the effect that the shrinking of the hard-scattered projectile nucleon has on the $dN^{\rm hard}/dQ$ distribution and brings the R_{p+A} and R_{CP} values closer to unity.

Our model predicts that for collisions of a projectile composed of N nucleons with a large nucleus, the modifications in the R_{p+A} and R_{CP} which result from proton color fluctuations will be diluted by a factor $1/N$ relative to p+A collisions, and that at fixed x_p the following

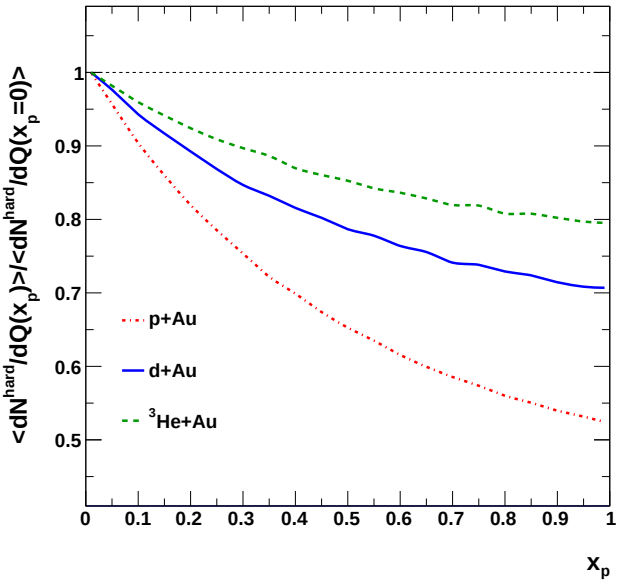

FIG. 5. (Color Online) The mean charge in the Au-going BBC for each collision system as a function of x_p, normalized to the value at $x_p = 0$.

ordering is expected,

Shrinking nucleon:

$$R^{\rm central}_{p+{\rm Au}} < R^{\rm central}_{d+{\rm Au}} < R^{\rm central}_{^3{\rm He}+{\rm Au}}. \qquad (12)$$

An inverted ordering would apply in the most peripheral collisions. On the other hand, if the modifications arise from an effect which grows with the amount of nuclear material in the collision (such as an initial- or final-state energy loss of hard-scattered partons in the nuclear medium), the opposite ordering may be expected,

Energy loss:

$$R^{\rm central}_{p+{\rm Au}} > R^{\rm central}_{d+{\rm Au}} > R^{\rm central}_{^3{\rm He}+{\rm Au}}. \qquad (13)$$

These competing descriptions of the data can be tested directly at RHIC with measurements of centrality-dependent hard-process rates in the recently-collected p+Au and ^{3}He+Au collision data.

Finally, since the modifications shown in Figs. 1 and 4 arise from an x_p-dependent modification of the centrality signal (which in PHENIX is the Au-going beam–beam counter charge, Q), an alternative but indirect way to explore this signature is by examining the mean value of Q in hard-scattered events as a function of x_p. In our model, this is given directly by the mean value of $dN^{\rm hard}/dQ(x_p)$. Figure 5 shows the dependence of the mean value of Q on x_p for all three collision systems. Since the overall scale of the mean charge is very different between the three systems, the results are plotted in ratio to the value at $x_p = 0$. Mathematically, this value is equal to the mean Q for hard-scattering events in the absence of an x_p-dependent shrinking of the projectile

nucleon. A clear hierarchy between the three systems is visible at each value of x_p, with the largest relative suppression at fixed x_p in p+Au collisions, and a systematically smaller reduction in the mean charge as additional nucleons are added to the projectile.

IV. DI-HADRON CORRELATIONS

The d+Au data analyzed in the previous section are from measurements of jet production at midrapidity which, along with our predictions, extends to the kinematic region $x_p \sim 0.4 - 0.5$. In the future, the large acceptance and hadronic calorimetry of the sPHENIX experiment [28], along with the projected performance for the luminosity of p+Au collisions at RHIC, will enable jet measurements at midrapidity which extend this range to $x_p \approx 0.75$. While our model is constrained by data in the region $x_p < 0.5$, it may be naturally extended to provide predictions at higher values as given by Eq. 4. Figure 6 shows that the predicted modifications increase continuously up to the kinematic limit $x_p = 1$.

In addition to these future measurements, the high-x_p region can also be accessed through measurements of hard-scattered yields at forward rapidity (downstream of the projectile beam, $y \gtrsim +2$). Such measurements have been previously performed in $\sqrt{s_{NN}} = 200$ GeV d+Au data by PHENIX [20, 21], STAR [22] and BRAHMS [23]. For our purposes, we focus on the PHENIX measurement of di-hadron production [21], since the centrality framework and selection is identical to that described in Sec. II. Particle production at moderate p_T in the forward region predominantly arises from collisions with low-x in the target (Au) nucleus, $x_{\rm Au} \lesssim 10^{-2}$. The measurement shows an increasing suppression in the quantity $J_{d+\rm Au}$, which is analogous to $R_{d+\rm Au}$ but for azimuthally balanced di-hadron pairs instead of single particles or jets, with decreasing $x_{\rm Au}$. This suppression has popularly been interpreted as arising from large, impact parameter dependent shadowing or parton saturation effects in the nuclear medium [29, 30], or from impact parameter dependent energy loss [31]. However, particle production in this kinematic region arises from parton–parton scatterings with large-x_p ($x_p > 0.1$) as well as small $x_{\rm Au}$, and the results are therefore sensitive to the physics of both, including the proton color fluctuation effects described in this paper (We note that the importance of the high-x_p kinematics has been previously raised in a different context by the authors of Ref. [32]).

In Ref. [21], centrality-dependent di-hadron yields were reported with two selections on kinematics: one hadron at midrapidity ($|\eta| < 0.35$) while the other hadron was at forward pseudorapidity ($3.1 < \eta < 3.8$), and also with both hadrons in the forward pseudorapidity region. In general, the latter selection is able to access lower $x_{\rm Au}$ and higher x_p values. Results were reported within different ranges of the leading and subleading hadron p_T, which were limited by kine-

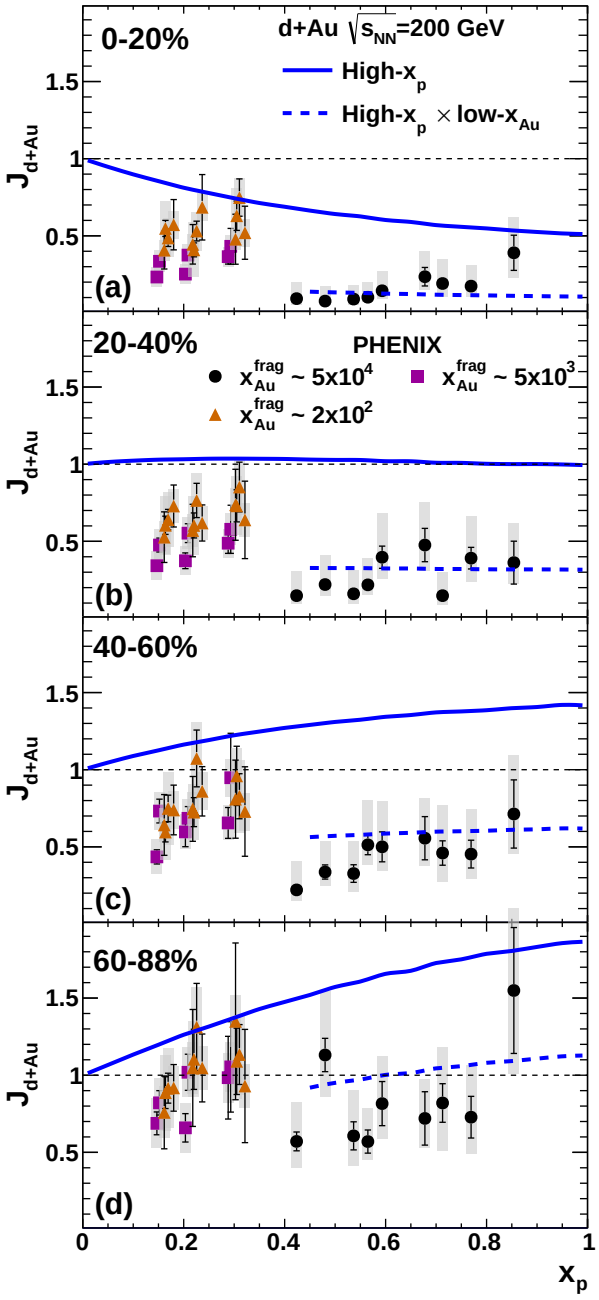

FIG. 6. (Color Online) The measured $J_{d+\rm Au}$ as a function of x_p [21] in each centrality bin compared to the calculated modification due to the shrinking projectile nucleon size in d+Au collisions.

matic considerations to 0.5—0.75, 0.75—1.0 and 1.0—1.5 GeV/c. To apply our framework to these results, di-hadron yields with a given pseudorapidity and p_T selection need to be associated with a specific value of x_p. PYTHIA [33] simulations were used to attempt to derive a mapping between the forward di-hadron kinematics and underlying value of x_p. However, in the simulation, string fragmentation processes without a tight association to the parton-parton kinematics contributed

significantly to the production of particles in this kinematic range. Thus, following Ref. [21], we estimate the mean x_p by assuming that the hadrons are the leading fragments of the outgoing hard-scattered partons in a leading order $2 \to 2$ picture,

$$x_p = \frac{\left[\left(p_{T,1}\exp(+\eta_1) + p_{T,2}\exp(+\eta_2)\right)/\langle z\rangle\right]}{\sqrt{s_{NN}}}, \qquad (14)$$

where $(p_{T,1}, p_{T,2})$ and (η_1, η_2) refer to the leading and subleading hadron p_T and pseudorapidity, and the typical fraction of the parton's p_T contained by the leading fragment is taken to be $\langle z\rangle = 0.6$.

The $J_{d+\mathrm{Au}}$ data are plotted as a function of estimated x_p, along with the results of our model calculation, in Fig. 6. For particle or jet production at fixed p_T, there is an anticorrelation between x_p and x_{Au}. However, the data in Fig. 6 are compiled from different selections on $p_{T,1}$ and $p_{T,2}$, complicating this relationship. Thus, the data points are plotted with different markers to distinguish three distinct ranges of x_{Au}.

In the most central (0–20%) collisions, the $J_{d+\mathrm{Au}}$ data show a substantially larger suppression than our calculation which incorporates only x_p-dependent proton color fluctuation physics. For data points arising from the smallest values of $x_{\mathrm{Au}} < 10^{-3}$, this difference is more than a factor of five. In the most peripheral collisions (60–88%), the data are at or slightly below unity, while the model predicts a substantial enhancement. Thus, our model substantially overpredicts the $J_{d+\mathrm{Au}}$ values in events of all centrality classes.

One possible explanation of this discrepancy is that assigning a definite value of x_p to this data is inappropriate. The d+Au di-hadron analysis assumes that the kinematics of the forward rapidity measurement is related to the initial parton–parton scattering kinematics x_p and x_{Au} in a well-defined way as described in Eq. 14. If such a correspondence does not apply for particle production at such low p_T, then the above comparison is likely invalid.

A second explanation is that additional physics effects must be accounted for. This is in striking contrast to the forward rapidity (up to $y \sim +4$) jet data in p+Pb collisions at the LHC which have a centrality dependent modification that is consistent with being only a function of x_p [2]. However, the p+Pb data are for reconstructed jets at much higher p_T values than those probed in the d+Au di-hadron measurement. Thus the differences may be attributable to the much lower momentum transfer scale Q^2 for the RHIC data.

An obvious candidate for an additional physics effect is the suppression of the parton density at low-x_{Au} described above. It notable that this effect would likely be very small for the p+Pb data at the LHC. This suppression would decrease the $J_{d+\mathrm{Au}}$ relative to the modifications arising from a high-x_p shrinking proton effect. This could provide the additional suppression by a factor of five in 0–20% collisions needed to describe the data. A similar but smaller low-x_{Au} suppression would also have to be present in peripheral events to explain the data. While it is commonly believed that peripheral d+Au events are similar to p+p collisions and contain no appreciable cold nuclear matter effects, measurements of quarkonia production [34, 35] found that even 60–88% d+Au collisions may have significant shadowing effects.

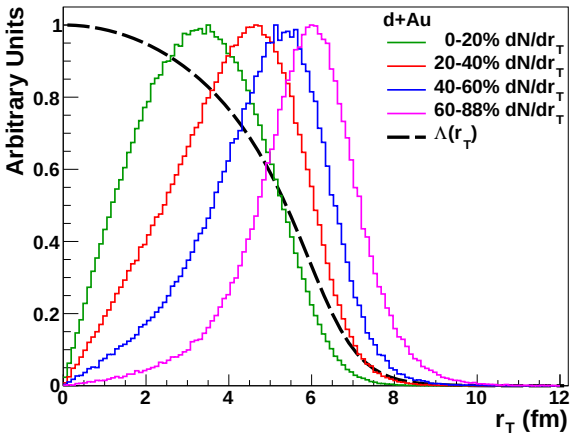

FIG. 7. Distributions of the radial impact position of nucleons (r_T) in d+Au collisions for each of the four PHENIX centrality bins, reproduced from Ref. [34]. Also shown is the nuclear thickness as a function of the impact position, in arbitrary units.

Ref. [34] calculates distributions of the projectile nucleon impact transverse radius, r_T, for each PHENIX d+Au centrality selection, using a MC-Glauber model combined with a parameterization of the PHENIX centrality detector effects. Figure 7 shows these distributions in four centrality selections. The distributions in each selection overlap substantially with one another, and the mean r_T between adjacent selections differs by typically less than 1 fm. Notably, the distribution in peripheral d+Au collisions has a mean of 5.7 fm (compared to 3.3 fm in central collisions), and a long tail towards small r_T values where the nucleus is thick.

We investigate if a small low-x_{Au} suppression in peripheral events can, in addition to the high-x_p effects, describe the data. To do this, we hypothesize that the centrality-dependent low-x_{Au} suppression effect can be parameterized as a linear function of the nuclear thickness,

$$J'_{d+\mathrm{Au}} = J_{d+\mathrm{Au}}\left(1 - cT_{p+A}\right), \qquad (15)$$

where $J_{d+\mathrm{Au}}$ contains the high-x_p effects, the parameter c encodes the strength of the centrality-dependent low-x_{Au} suppression effects, and $J'_{d+\mathrm{Au}}$ contains both high-x_p and low-x_{Au} effects together. If c is chosen to produce the factor of $J'_{d+\mathrm{Au}}/J_{d+\mathrm{Au}} = 0.2$ for $x_p > 0.4$ in central events, Eq. 15 predicts a suppression of $J'_{d+\mathrm{Au}}/J_{d+\mathrm{Au}} = 0.6$ for peripheral events in this region of x_p.

Figure 6 shows the calculated $J'_{d+\mathrm{Au}}$, which agrees well with the data in the region $x_p > 0.4$ for each central-

ity selection. Thus, the centrality-dependence of hadron production at forward rapidity in d+Au collisions is consistent with a combination of effects from proton color fluctuations at high-x_p and an additional suppression from low-$x_{\rm Au}$ effects linear in the nuclear thickness.

This analysis is not meant to replace a more detailed calculation of impact parameter dependent low-$x_{\rm Au}$ effects, but instead is meant to highlight that with a very strong physics effect in central events, one may naturally expect a smaller, but still significant, effect in peripheral events. Proton color fluctuations effects, which may be logically expected from the midrapidity data, also play a role in this kinematic region at low-$x_{\rm Au}$.

A better understanding of the relevant physics effects can be achieved with a comparable di-hadron measurement in p+Au collisions. In this system, cold nuclear matter shadowing effects would be very similar to those in d+Au collisions. However, as we have argued in Sec III, the high-x_p effects would be substantially larger, allowing for the separation of the two effects through the analysis of both collision systems.

V. SUMMARY

This paper presents a simple geometric model of an x_p-dependent decrease in the interaction strength of the hard-scattered projectile nucleon in $p/d/^3$He+Au collisions. We implement this shrinking-nucleon picture using a MC-Glauber approach and calculate the resulting nuclear modification factors for centrality-dependent hard-scattering yields. After tuning, our one-parameter description of the x_p-dependence successfully describes the full p_T and centrality dependence of the measured $R_{d+\rm Au}$ and R_{CP} values for midrapidity jet production in d+Au collisions at $\sqrt{s_{NN}} = 200$ GeV.

Having tuned our model to d+Au collisions, we make quantitative predictions for p_T and centrality dependent nuclear modification factors in p+Au and ^{3}He+Au collisions. We find that the one fewer (one additional) nucleon in p+Au (^{3}He+Au) collisions results in systematically larger (smaller) modifications arising from the shrinking of the projectile nucleon configurations with a large-x_p parton, relative to d+Au collisions. This results in a clear ordering of the calculated $R_{p+\rm A}$ and R_{CP} values based on projectile mass in the three collision systems. Recently collected data in these systems at RHIC can quantitatively test this picture. In particular, measurements of high-p_T jet or neutral pion production at midrapidity can distinguish the predicted $> 50\%$ differences in the most central to most peripheral R_{CP} ratio at $x_p \sim 0.3$.

We also explore the relevance of the shrinking nucleon configurations with a large-x_p parton for previous measurements of centrality-dependent di-hadron production in d+Au collisions at forward rapidity. We find that while this large-x_p effect contributes to measurements in this kinematic regime, it alone does not provide a complete description of that data, with the additional modifications presumably arising from low-$x_{\rm Au}$ shadowing, saturation or energy loss effects in the nuclear medium. However, we demonstrate that the high-x_p effects must be taken into account to properly determine the impact parameter dependence of the low-$x_{\rm Au}$ or energy loss effects. Finally, we argue that an analogous measurement in p+Au collisions, where the low-$x_{\rm Au}$ physics should be unchanged but the large-x_p physics more impactful, can further clarify the picture.

ACKNOWLEDGMENTS

DM and JLN acknowledge funding from the Division of Nuclear Physics of the U.S. Department of Energy under Grant No. DE-FG02-00ER41152. DVP acknowledges funding from the U.S. Department of Energy under Contract No. DE-SC0012704. DVP also acknowledges Mark Strikman for useful discussions.

[1] A. Adare *et al.* (PHENIX), (2015), arXiv:1509.04657 [nucl-ex].
[2] G. Aad *et al.* (ATLAS), Phys. Lett. **B748**, 392 (2015), arXiv:1412.4092 [hep-ex].
[3] K. J. Eskola, H. Paukkunen, and C. A. Salgado, JHEP **04**, 065 (2009), arXiv:0902.4154 [hep-ph].
[4] Z.-B. Kang, I. Vitev, and H. Xing, Phys. Rev. **C92**, 054911 (2015), arXiv:1507.05987 [hep-ph].
[5] M. L. Miller, K. Reygers, S. J. Sanders, and P. Steinberg, Ann. Rev. Nucl. Part. Sci. **57**, 205 (2007), arXiv:nucl-ex/0701025 [nucl-ex].
[6] A. Bialas, M. Bleszynski, and W. Czyz, Nucl. Phys. **B111**, 461 (1976).
[7] A. Adare *et al.* (PHENIX), Phys. Rev. **C90**, 034902 (2014), arXiv:1310.4793 [nucl-ex].
[8] G. Aad *et al.* (ATLAS), (2015), arXiv:1508.00848 [hep-ex].
[9] X. Zhang and J. Liao, (2013), arXiv:1311.5463 [nucl-th].
[10] I. Helenius, K. J. Eskola, H. Honkanen, and C. A. Salgado, JHEP **07**, 073 (2012), arXiv:1205.5359 [hep-ph].
[11] G. Aad *et al.* (ATLAS), Phys. Lett. **B756**, 10 (2016), arXiv:1512.00197 [hep-ex].
[12] D. V. Perepelitsa and P. A. Steinberg, (2014), arXiv:1412.0976 [nucl-ex].
[13] J. Adam *et al.* (ALICE), Phys. Rev. **C91**, 064905 (2015), arXiv:1412.6828 [nucl-ex].
[14] H. Heiselberg, G. Baym, B. Blaettel, L. L. Frankfurt, and M. Strikman, Phys. Rev. Lett. **67**, 2946 (1991).
[15] B. Blaettel, G. Baym, L. L. Frankfurt, H. Heiselberg, and M. Strikman, Phys. Rev. **D47**, 2761 (1993).
[16] S. J. Brodsky and G. R. Farrar, Phys. Rev. Lett. **31**, 1153 (1973).
[17] M. Alvioli, B. A. Cole, L. Frankfurt, D. V. Perepelitsa, and M. Strikman, Phys. Rev. **C93**, 011902 (2016),

arXiv:1409.7381 [hep-ph].
[18] N. Armesto, D. C. Gülhan, and J. G. Milhano, Phys. Lett. **B747**, 441 (2015), arXiv:1502.02986 [hep-ph].
[19] A. Bzdak, V. Skokov, and S. Bathe, (2014), arXiv:1408.3156 [hep-ph].
[20] S. S. Adler *et al.* (PHENIX), Phys. Rev. Lett. **94**, 082302 (2005), arXiv:nucl-ex/0411054 [nucl-ex].
[21] A. Adare *et al.* (PHENIX), Phys. Rev. Lett. **107**, 172301 (2011), arXiv:1105.5112 [nucl-ex].
[22] B. I. Abelev *et al.* (STAR), (2007), arXiv:nucl-ex/0703016 [nucl-ex].
[23] I. Arsene *et al.* (BRAHMS), Phys. Rev. Lett. **93**, 242303 (2004), arXiv:nucl-ex/0403005 [nucl-ex].
[24] C. Loizides, J. Nagle, and P. Steinberg, (2014), arXiv:1408.2549 [nucl-ex].
[25] P. Hodgson, *Nuclear Reactions and Nuclear Structure* (Clarendon Press, 1971).
[26] Analogous values for p+Au and ^{3}He+Au collisions were provided by the PHENIX Collaboration.
[27] M. Alvioli, H. J. Drescher, and M. Strikman, Phys. Lett. **B680**, 225 (2009), arXiv:0905.2670 [nucl-th].
[28] A. Adare *et al.* (PHENIX), (2015), arXiv:1501.06197 [nucl-ex].
[29] A. Stasto, B.-W. Xiao, and F. Yuan, Phys. Lett. **B716**, 430 (2012), arXiv:1109.1817 [hep-ph].
[30] A. Dumitru, J. Jalilian-Marian, T. Lappi, B. Schenke, and R. Venugopalan, Phys. Lett. **B706**, 219 (2011), arXiv:1108.4764 [hep-ph].
[31] Z.-B. Kang, I. Vitev, and H. Xing, Phys. Rev. **D85**, 054024 (2012), arXiv:1112.6021 [hep-ph].
[32] B. Z. Kopeliovich, J. Nemchik, I. K. Potashnikova, M. B. Johnson, and I. Schmidt, Phys. Rev. **C72**, 054606 (2005), arXiv:hep-ph/0501260 [hep-ph].
[33] T. Sjostrand, S. Mrenna, and P. Z. Skands, JHEP **0605**, 026 (2006), arXiv:hep-ph/0603175 [hep-ph].
[34] A. Adare *et al.* (PHENIX), Phys. Rev. Lett. **107**, 142301 (2011), arXiv:1010.1246 [nucl-ex].
[35] D. C. McGlinchey, A. D. Frawley, and R. Vogt, Phys. Rev. **C87**, 054910 (2013), arXiv:1208.2667 [nucl-th].